Increased FGF21 in brown adipose tissue of tyrosine hydroxylase heterozygous mice: implications for cold adaptation[S]

Patricia Vázquez,[1,*,†,§] Catalina Hernández-Sánchez,[†,§] Carmen Escalona-Garrido,[*,§] Laura Pereira,[§,] Cristina Contreras,[††] Miguel López,[§§,***] Jesús Balsinde,[§,**] Flora de Pablo,[†,§] and Ángela M. Valverde[1,§,*]**

Alberto Sols Biomedical Research Institute (IIBm),* Consejo Superior de Investigaciones Científicas/Universidad Autónoma de Madrid (CSIC/UAM), Madrid, Spain; Centro de Investigaciones Biológicas,[†] Consejo Superior de Investigaciones Científicas, (CSIC) Madrid, Spain; Centro de Investigación Biomédica en Red de Diabetes y Enfermedades Metabólicas (CIBERdem),[§] Instituto de Salud Carlos III, Madrid, Spain; Instituto de Biología y Genética Molecular,** Consejo Superior de Investigaciones Científicas (CSIC), Universidad de Valladolid, Valladolid, Spain; Physiology Department,[††] Pharmacy School, Complutense University of Madrid, Madrid, Spain; NeurObesity Group,[§§] Department of Physiology, Centro Singular de Investigación en Medicine Molecular y Enfermedades Crónicas (CIMUS), University of Santiago de Compostela, Instituto de Investigación Sanitaria, Santiago de Compostela, Spain; and Centro de Investigación Biomédica en Red Fisiopatología de la Obesidad y Nutrición (CIBERobn),*** Santiago de Compostela, Spain

Abstract **Tyrosine hydroxylase (TH) catalyzes the first step in catecholamines synthesis. We studied the impact of reduced TH in brown adipose tissue (BAT) activation. In adult heterozygous ($Th^{+/-}$) mice, dopamine and noradrenaline (NA) content in BAT decreased after cold exposure. This reduced catecholaminergic response did not impair cold adaptation, because these mice induced uncoupling protein 1 (UCP-1) and maintained BAT temperature to a similar extent than controls ($Th^{+/+}$). Possible compensatory mechanisms implicated were studied. *Prdm16* and *Fgf21* expression, key genes in BAT activation, were elevated in $Th^{+/-}$ mice at thermoneutrality from day 18.5 of embryonic life. Likewise, plasma FGF21 and liver *Fgf21* mRNA were increased. Analysis of endoplasmic reticulum (ER) stress, a process that triggers elevations in FGF21, showed higher phospho-IRE1, phospho-JNK, and CHOP in BAT of $Th^{+/-}$ mice at thermoneutrality. Also, increased lipolysis in BAT of cold-exposure $Th^{+/-}$ mice was demonstrated by increased phosphorylation of hormone-sensitive lipase (HSL), as well as diacylglycerol (DAG) and FFA content.[F1r] Overall, these results indicate that the mild effects of *Th* haploinsufficiency on BAT function are likely due to compensatory mechanisms involving elevations in *Fgf21* and *Prdm16* and through adaptive changes in the lipid profile.**—Vázquez, P., C. Hernández-Sánchez, C. Escalona-Garrido, L. Pereira, C. Contreras, M. López, J. Balsinde, F. de Pablo, and Á. M. Valverde. **Increased FGF21 in brown adipose tissue of tyrosine hydroxylase heterozygous mice: implications for cold adaptation.** ***J. Lipid Res.*** **2018.** 59: **2308–2320.**

Supplementary key words catecholamines • diabetes • fatty acids • metabolic disease • obesity • fibroblast growth factor 21

Obesity is an important global health problem that results from an imbalance between energy intake and expenditure (1). Three types of adipose cells (white, brown, and beige) have been described with different developmental origins, cell-specific gene expression, and distinct functions (2). Whereas white adipocytes accumulate energy in the form of triglyceride depots that are distributed in a large fat droplet and contain few mitochondria, brown

This work was supported by Ministry of Science, Technology and Innovation Grants BFU 2010-15868 (to F.d.P. and C.H-S.), SAF2015-73000-EXP and SAF2016-80883 (to J.B.), and SAF2015-65267-R (to A.M.V.). The authors also acknowledge Instituto de Salud Carlos III Grant INFLAMES PIE14/00045 (cofunded by European Regional Development Fund "Investing in your Future") (to A.M.V.) and Centro de Investigación Biomédica en Red de Diabetes y Enfermedades Metabólicas Asociadas. This is an initiative of the Instituto de Salud Carlos III. The authors acknowledge Ministerio de Ciencia e Innovación-Consejo Superior de Investigaciones Científicas and the European Social Fund for the JAE-DOC contract (2013 to P.V.) and a Centro de Investigación Biomédica en Red de Diabetes y Enfermedades Metabólicas Asociadas contract (2016 to P.V.).

Manuscript received 20 March 2018 and in revised form 10 October 2018.

Published, JLR Papers in Press, October 23, 2018
DOI https://doi.org/10.1194/jlr.M085209

Abbreviations: BAT, brown adipose tissue; CE, cholesteryl ester; DiO2, deiodinase 2; e18.5, embryonic day 18.5; ER, endoplasmic reticulum; FGF21, fibroblast growth factor 21; HSL, hormone-sensitive lipase; iWAT, inguinal white adipose tissue; NA, noradrenaline; TAG, triacylglycerol; TH, tyrosine hydroxylase; UCP-1, uncoupling protein 1; WAT, white adipose tissue.

[1]To whom correspondence should be addressed.
e-mail: patrivazquez@iib.uam.es (P.V.); avalverde@iib.uam.es (Á.M.V.)

[S] The online version of this article (available at http://www.jlr.org) contains a supplement.

adipocytes present multilocular fat droplets and contain a higher number of mitochondria (3). Brown adipocytes are responsible for nonshivering thermogenesis by uncoupling the proton gradient generated by oxidative phosphorylation and ATP synthesis, due to the specific expression of the uncoupling protein 1 (UCP-1) in the inner mitochondrial membrane. This brings out energy dissipation as heat (4). Recently, a third class of adipocytes has been identified and termed "beige" or "brite" adipose cells. They reside within white adipose tissue (WAT), but can acquire characteristics of brown adipocytes under different environmental or pharmacological stimuli (5, 6).

It is known that brown adipose tissue (BAT), which is maintained in adult humans (7), uses glucose and FAs as fuel (8), and its activity is reduced in obese and diabetic individuals (1). For this reason, understanding the mechanisms involved in the control of BAT activity could lead to improving the treatment of these patients. BAT is a highly vascularized and innervated tissue (9). Classical activation of thermogenesis occurs via noradrenaline (NA) released from the sympathetic nervous system, which binds to β3 adrenergic receptors (*Adrb3*) present in the brown adipocyte. Receptor activation increases intracellular cAMP, which induces lipolysis, leading to the release of FFAs that, in turn, activate UCP-1. In fact, the surgical denervation of interscapular BAT reduced the activation of brown adipocytes after cold exposure (10).

Tyrosine hydroxylase (TH) catalyzes the first and rate-limiting step in the synthesis of catecholamines. A null mutation in the mouse *Th* gene causes a depletion of catecholamines and lethality at prenatal stages because of cardiovascular failure (11–13). Additionally, this mutation has an impact on pancreatic β-cell development (14). Recently, it was reported that haploinsufficiency of *Th* increases mouse half-life by protecting against age-associated hypertension (15). In contrast, patients with pheochromocytomas that produce and secrete large amounts of catecholamines (NA or adrenaline) present body weight loss, among other abnormalities (16). The importance of the sympathetic stimulation in BAT for cold adaptation has also been shown because adrenal medullar TH is involved in the response to stress induced by cold (17). More recently, a role of TH on the antiinflammatory responses triggered by cold exposure has been reported (18).

BAT is also a secretory tissue that releases different molecules (batokines) with autocrine and paracrine roles (19). One of these batokines is the fibroblast growth factor 21 (FGF21), which was initially identified as a hepatokine and is considered, rather than a mitogenic factor, an atypical FGF due to its role in endocrine function over carbohydrates and FA metabolism (20). *Fgf21*-null mice have reduced hepatic FA oxidation and a concomitant increase in liver fat accumulation (21). More recently, it has been demonstrated that FGF21 is highly produced and released by BAT after cold exposure (19). FGF21 also impacts "browning" of WAT, and, as a consequence, it can improve lipid metabolic disorders and insulin resistance (22).

In this study, we examined how *Th*-haploinsufficiency in mice affects the response to the stress induced by cold exposure in BAT. Our data show that, despite reduced catecholamine levels, *Th*-haploinsufficiency does not impair cold adaptation in mice. We also demonstrate that this unaltered adaptive response is associated with increased FGF21 and increased lipolytic capacity in BAT. This evidence suggests a new mechanism for cold adaptation in a context of low adrenergic signaling.

MATERIALS AND METHODS

Animal procedures

All procedures involving animals were approved by the Ethics Committee of Consejo Superior de Investigaciones Científicas and Comunidad de Madrid in accordance with the European Union guidelines. The C57BL6/J *Th* heterozygote mouse strain was kindly provided by R. D. Palmiter (University of Washington, Seattle, WA) (12). All the studies were performed using littermates. We used three groups named adult mice (2–3 months), embryos at embryonic day (e) 18.5, and aged mice (15 months). The animals were maintained on 12 h:12 h light-dark cycles and at 22°C and allowed free access to standard rodent chow and water ad libitum. The adult mice were randomly divided into two experimental groups: One group was maintained at thermoneutral conditions (29°C), and the other one was subjected to cold challenge (4°C) for 6 h. Prior to the cold exposure, the two groups of mice were housed at 29°C for at least 1 week. Body weight and rectal temperature were measured in all mice before and after cold exposure.

Preparation of tissue extracts and Western blot

BAT samples were homogenized at 4°C in lysis buffer (in mmol/l: 50 Tris HCl, 2 EGTA, 10 EDTA, 2 orthovanadate, 50 NaF, and 1 sodium pyrophosphate) containing 1% (w/v) Triton X-100 and a mini EDTA-free protease inhibitor tablet. Samples were homogenized in lysis buffer using The Brinkmann Pt 10/35 Polytron. Tissue lysates were centrifuged at 20,000 *g* for 30 min at 4°C, and the supernatants were collected and stored at −80°C until further analysis. Total protein extracts (15–30 μg) were loaded into Any kD Criterion TGX Precast Gels (catalog no. 567-1124, Bio-Rad, CA) and transferred onto PVDF membranes (catalog no. 170-4157, Bio-Rad) for 14 min at 25 V using a Trans-Blot Turbo Transfer System (Bio-Rad). Membranes were activated with 100% methanol for 2 min and blocked for 1 h at room temperature with 5% (w/v) BSA or nonfat milk in TBS-Tween 20 (0.05% w/v) and incubated overnight at 4°C with primary Abs: anti-TH (1:500) (Millipore, AB 152), anti-β-III tubulin (1:500) (covance MRB 435P), anti-CHOP [1:4,000, GADD153(R-20) sc-793], anti-pJNK (1:4,000, Cell Signaling 9251S), anti-JNK (1:1,000, Santa Cruz, SC-571), anti-pIRE (1:1,000 NB100-2323), anti-pHSL-s660 (1:1,000, Cell Signaling 4126S), and anti-HSL (1:1,000, Cell Signaling 4107S). After washing, the membranes were reblotted with anti-β-actin (1:5,000) (Sigma, St. Louis, catalog no. A5316), anti-tubulin (1:2,000) (Sigma, T4026), or vinculin (7F9) (1:25,000) (Santa Cruz, 73614) Abs as loading controls. Additionally, we used Ponceau Red as a loading control (Sigma). Abs were detected with the corresponding HRP-labeled secondary Abs (Pierce, Rockford, IL) and visualized with the Super Signal West Pico chemiluminescent substrate (Pierce). Different experiments were quantified by scanning densitometry using ImageJ software.

RNA isolation and quantitative real-time PCR

Total RNA from BAT, inguinal WAT (iWAT), or liver was extracted using TRIzol reagent, and reverse transcription was

performed using the High-Capacity cDNA Reverse Transcription Kit (Applied Biosystems, Waltham, MA) using random primers and Superscript III enzyme according to the manufacturer's instructions. Quantitative real-time PCR was performed in a 7900 HT-Fast real-time PCR (Life Technologies) with SYBR or Taqman Universal PCR Master Mix. The following probes and primers are listed in **Table 1**. Results are expressed using the $2^{-\Delta\Delta Ct}$ (cycle threshold) quantification method. Results were normalized according to expression levels of *Tbp* or *Rlbp0* RNA.

Immunohistochemistry

For immunohistochemical analysis, a piece of BAT was fixed overnight at 4°C in 4% (w/v) paraformaldehyde, then rinsed with PBS and dehydrated through an ethanol gradient before embedding in paraffin for microtome sectioning. Paraffin sections (7–8 μm) were dewaxed in Histo-Clear-II (CONDA, Madrid, Spain) and rehydrated through a descending series of ethanol dilutions. Antigen retrieval was achieved by microwaving [twice for 5 min at 600 W in 0.01 mmol/l citrate buffer (pH 6) with 0.05% (w/v) Tween-20] followed by three washes in PBS. Tissue sections were permeabilized with PBS-Triton X-100 (2% w/v). Nonspecific binding was blocked with 3% (v/v) donkey immunoserum (Sigma, Diegen, Belgium) in PBS-Triton X-100 (1% w/v). Sections were incubated overnight at 4°C with primary Abs (1:100) in blocking buffer and then incubated with secondary Abs labeled with either Alexa 568 or Alexa 647 dyes (1:250) (Molecular Probes, Carlsbad, CA). Nuclei were labeled with 4',6-diamidino-2-phenylindole (DAPI) (Molecular Probes). Images were collected by confocal microscopy (Leica TCS-SP5; Leica Microsystems, Wetzlar, Germany). H&E staining was performed in paraffin sections of BAT of $Th^{+/+}$ and $Th^{+/-}$ mice for morphological analysis. Images were collected with an Axiophot light microscope (Zeiss) with a 40× objective. To estimate the size of the lipid droplets, we used ImageJ software (The National Institutes of Health; https://imagej.nih.gov/ij/). First, the color images were converted to black and white images and then inverted. The percentage of white area versus area total was calculated. To estimate the cell density, we counted the nuclei per section in at least 10 fields of different 5 μm BAT sections of each animal. Around 2,000 total nuclei per mouse were counted.

ELISA

Catecholamines were determined by ELISA (3-CAT research ELISA, BA E-5600 LDN, Nordhorn, Germany) following the manufacturer's instructions. One piece of BAT of each animal was homogenized in buffer (0.01 N HCl, 1 mM EDTA, and 4 mM $Na_2S_2O_5$), and following centrifugation at 17,949 *g* for 15 min at 4°C, the supernatants were collected and stored at −80°C. All measurements were normalized by protein concentration. FGF21 plasma levels were quantified by ELISA (catalog no. RD291108200R, BioVendor) following the manufacturer's instructions.

In vitro experiments

The immortalized brown preadipocyte cell line was generated from mouse interscapular BAT and fully differentiated to brown adipocytes following the protocol previously described (23). Cells (day 7 of differentiation) were incubated with or without 1 μg/ml recombinant FGF21 (catalog no. RD272108100-B, BioVendor) for 18 h. Then, cells were treated with 0.1 μM NA for a further 4 h. After washing with PBS, cells were lysed in lysis buffer (10 mM Tris-HCl, 5 mM EDTA, 50 mM NaCl, 1% Triton X-100, 30 mM sodium pyrophosphate, 50 mM fluoride, 1 mM phenylmethanelsulfonyl fluoride, and 10 μg/ml protease inhibitors, pH 7.4–7.6). After centrifugation at 12,000 *g* for 7 min at 4°C, the total protein in supernatants was quantified with the BCA Protein Assay Kit. The phosphorylation of HSL (Ser-660) and UCP-1 protein levels were analyzed by Western blot using vinculin (7F9) (1:25,000) (Santa Cruz, catalog no. 73614) as a loading control. The amount of glycerol released by the cells to the culture medium after the different treatments was analyzed using a commercial kit (F628, Sigma).

Analysis of FFAs and triacylglycerol levels

Plasma glycerol levels were quantified using a commercial kit (catalog no. F6428, Sigma) and plasma nonesterified ("free" or unsaturated) FAs (FFAs) were quantified using commercial kits (catalog nos. 919898, 91696, and 91096, WAKo Chemicals, Richmond, VA), according to the manufacturer´s instructions. Samples were normalized by protein concentration.

Lipidomic analysis

Total lipids from BAT were extracted according to Folch et al. (24). Lipid classes were separated by TLC. For neutral lipid separation, a solvent mixture consisting of *n*-hexane/diethyl ether/acetic acid (70:30:1, v/v/v) was used as the mobile phase (25). The various neutral lipid classes cholesteryl esters (CEs), triacylglycerol

TABLE 1. Primer sequences and Taqman probes used in real-time PCR

Gene	Forward	Reverse	Taqman Probe
Atf2	5′-CCGTTGCTATTCCTGCATCAA-3′	5′-TTGCTTCTGACTGGACTGGTT-3′	
Ppara	5′-AGAGCCCCATCTGTCCTCTC- 3′	5′-ACTGGTAGTCTGCAAAACCAAA-3′	
Rplp0(364B)	5′-ACTGGTCTAGGACCCGAGAAG-3′	5′-TCCCACCTTGTCTCCAGTCT-3′	
Adrb3			Mm02601819_g1
Adipoq			Mm00456425_m1
Agr1			Mm00475988_m1
β *klotho*			Mm00473122_m1
Bmp8b			Mm00432115_g1
Cebpa			Mm00514283_s1
Cidea			Mm00432554_m1
Cox8b			Mm00432648_m1
Cpt1a			Mm01231183_m1
Dio2			Mm00515664_m1
Fgf21			Mm00840165_g1
Fgfr1			Mm00438930_m1
Nos2			Mm00440502_m1
Pparg			Mm00440940_m1
Ppargc1a			Mm01208835_m1
Prdm16			Mm00712556_m1
Tbp			Mm00446971_m1
Ucp1			Mm01244861_m1

(TAG), diacylglycerol (DAG), and FFAs were scraped and extracted from the silica with 1 ml of chloroform/methanol (1:2, v/v) followed by 1 ml of chloroform/methanol (2:1, v/v). The CE, TAG, and DAG fractions were treated with 500 µl of 0.5 M KOH in methanol for 60 min at 37°C to obtain FA methyl esters. To neutralize, 500 µl of 0.5 M HCl was added. The FFA fraction was treated with 450 µl of MeOH in 0.5% HCl for 20 min at 45°C, and neutralized with one vol of 0.14 M KOH and 500 µl of deionized water was added. Extraction of the FA methyl esters was carried out with 2 ml of *n*-hexane, and 1 µl was subjected to GC/MS analysis as previously described (26, 27), using an Agilent 7890A gas chromatograph coupled to an Agilent 5975C mass-selective detector operated in electron impact mode (EI, 70 eV), equipped with an Agilent 7693 autosampler and an Agilent DB23 column (60 m length × 0.25 mm internal diameter × 0.15 µm film thickness). Data analysis was carried out with the Agilent G1701EA MSD Productivity Chemstation software, revision E.02.00.

Measurement of skin temperature surrounding BAT

The skin temperature surrounding BAT was recorded with an infrared camera (B335:Compact-Infrared-Thermal-Imaging-Camera; FLIR; West Malling, Kent, UK) and analyzed with a specific software package (FLIR-Tools-Software; FLIR), as previously shown (28, 29). Pictures were taken at both thermoneutral conditions or immediately after cold exposure (6 h).

Indirect calorimetry

Th$^{+/+}$ *and Th*$^{+/-}$ mice at 2–3 months of age were individually housed and maintained at thermoneutrality (28–29°C) under a 12:12 h light-dark cycle in a Phenomaster system (TSE Systems, Bad Homburg, Germany). Food and water were provided ad libitum in the appropriated devices. Mice were acclimated to the chambers for at least 24 h and then monitored for an additional 48 h period. After that, mice were placed into the cold room (4°C) for 6 h and then immediately moved to their original cages of the TSE system to continue the measurement for additional 24 h.

Statistical analysis

Statistical analyses were performed using a Student's *t*-test, a nonparametric test (Mann-Whitney *U* test), or two-way ANOVA with Bonferroni's post hoc test. All statistical analyses were performed with GraphPad Prism software version 5 (GraphPad Software, Inc., San Diego, CA). Statistical significance was set at * $P < 0.05$, ** $P < 0.01$, and *** $P < 0.001$, *Th*$^{+/-}$ versus *Th*$^{+/+}$ groups; and $^{\#}P < 0.05$, $^{\#\#}P < 0.01$, and $^{\#\#\#}P < 0.001$, 4°C versus 29°C groups.

RESULTS

Characterization of BAT in *Th*$^{+/+}$ and *Th*$^{+/-}$ mice at thermoneutrality

We first characterized adult (3 month old) *Th*$^{+/-}$ and *Th*$^{+/+}$ mice at thermoneutral conditions (29°C). As shown in **Fig. 1A**, no differences between the two genotypes of mice were found in body weight and rectal temperature. Likewise, temperature of skin surrounding BAT, energy expenditure, and respiratory exchange ratio were similar in the two genotypes (Fig. 1B and supplemental Fig. S1). As expected, Western blot analysis revealed a 50% decrease of TH protein content in the BAT of *Th*$^{+/-}$ mice compared with levels of their *Th*$^{+/+}$ littermates (Fig. 1C). The analysis of paraffin sections showed reduced TH-positive immunostaining

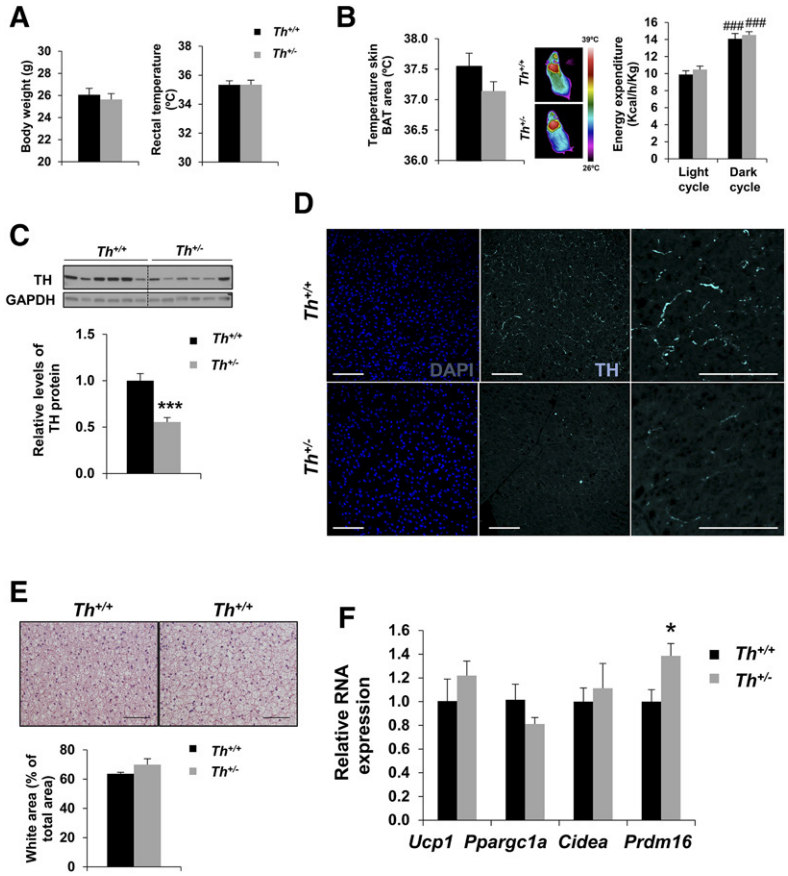

Fig. 1. Characteristics of *Th*$^{+/-}$ mice in thermoneutrality. Body weight and rectal temperature (A), skin temperature surrounding BAT, and energy expenditure (B) were measured in *Th*$^{+/+}$ and *Th*$^{+/-}$ mice housed 1 week at 29°C. C: Western blot analysis and quantification of lysates from BAT collected from *Th*$^{+/+}$ and *Th*$^{+/-}$ adult mice showing TH levels using GAPDH as a loading control. D: Representative immunohistochemistry of TH at paraffin sections. Nuclei were stained with DAPI (blue) and TH+ fibers were detected by immunostaining (cyan). E: Representative sections of BAT from *Th*$^{+/+}$and *Th*$^{+/-}$ mice stained with H&E and quantification of the percentage of white area versus total area. F: Quantitative RT-PCR of thermogenic gene expression in BAT. The graph represents the relative gene expression compared with *Th*$^{+/+}$ mice. The data were normalized by *Tbp* RNA expression. Data are mean ± SEM. n = 5–10/group in A–C, n = 5–7/group in E, and n = 4–10/group in F. Mann-Whitney *U* test was used. *$P < 0.05$; ***$P < 0.001$ (between *Th*$^{+/+}$ and *Th*$^{+/-}$ mice); ###$P < 0.001$ (between each genotypes in dark cycle versus light cycle). Scale bars: 75 µm.

in the BAT of $Th^{+/-}$ mice (Fig. 1D), although no major differences were observed in the amount of innervating fibers, as shown by Western blot and immunohistochemistry for β-III-tubulin (supplemental Fig. S2A, B). H&E staining revealed similar BAT histology in $Th^{+/-}$ and $Th^{+/+}$ mice (Fig. 1E), although a slight increase in white area (Fig. 1E) and decreased cell density (supplemental Fig. S2C) was found in $Th^{+/-}$ mice. We next analyzed the expression of some key genes for BAT identity. Whereas the expression of thermogenic-related genes such as *Ucp1*, *Ppargc1a* (which encodes PGC1α), and *Cidea* was similar between the two genotypes, the levels of *Prdm16*, a relevant gene in brown fat adipogenesis, were significantly higher in the $Th^{+/-}$ mice than in their WT littermates (Fig. 1F). Further characterization of BAT-related gene expression showed no differences between the two genotypes of mice at thermoneutral conditions (supplemental Fig. S2D).

$Th^{+/-}$ mice responded normally to cold exposure

Next, we addressed a possible impact of reduced TH expression in cold adaptation in young mice at 3 months of age. After 6 h of cold exposure (4°C), the BAT of $Th^{+/-}$ mice maintained lower TH protein levels than their WT littermates (supplemental Fig. S3A). Concordantly, dopamine and NA content, determined by ELISA, were diminished in BAT of $Th^{+/-}$ mice after 6 h of cold exposure (**Fig. 2A**). Similar to thermoneutrality, H&E-stained sections revealed more white area in $Th^{+/-}$ compared with $Th^{+/+}$ mice after cold exposure (supplemental Fig. S3B). Surprisingly, body weight (Fig. 2B), rectal temperature, and temperature of skin surrounding BAT (Fig. 2C, D), all indicators of cold adaptation, were similar in both genotypes of mice. Moreover, energy expenditure was elevated in $Th^{+/-}$ mice immediately after cold exposure and also during the following night period (Fig. 2E). Notably, despite the impaired catecholamine production, the expression of *Ucp1* and *Ppargc1a* was similarly increased in $Th^{+/-}$ and $Th^{+/+}$ mice upon cold challenge (Fig. 2F, G). It has been previously reported that cold exposure does not modify RNA expression levels of *Prdm16* and *Cidea* (30). In agreement with these results, no differences were found in either $Th^{+/+}$or $Th^{+/-}$ mice (Fig. 2H, I), although *Prdm16* levels, which were elevated at 29°C in the $Th^{+/-}$ mice, decreased to levels of the $Th^{+/+}$ mice after cold exposure (Fig. 2H). Body weight, rectal temperature, and the expression of *Ucp1* and *Ppargc1a* remained similar in both genotypes after more prolonged (16 h) cold exposure (supplemental Fig. S4). These results indicate that reduction of catecholamine levels does not alter the BAT acute response to cold. Notably, this effect was unrelated to compensatory changes in adrenergic signaling, because no differences between both genotypes were found in *Adrb3* RNA at basal conditions. Indeed, *Adrb3* RNA levels decreased similarly in both groups of mice after cold challenge (supplemental Fig. S5A), as reported (31–33).

Besides UCP-1, BAT thermogenesis relies on deiodinase 2 (DiO2) enzymatic activity (34). The conversion of T4 into

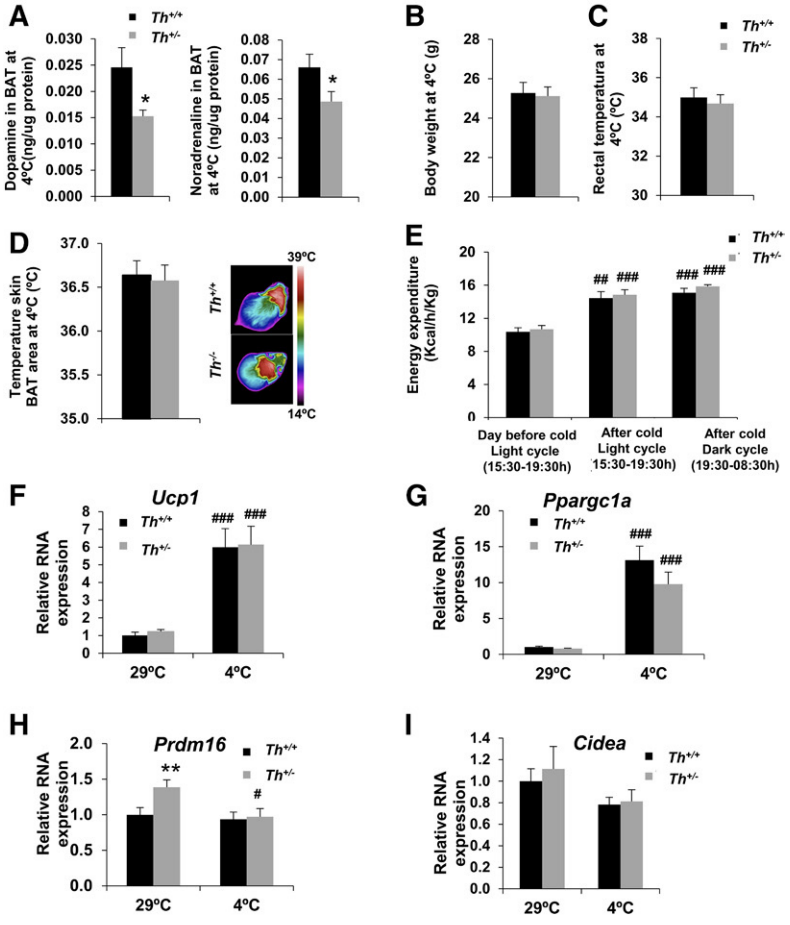

Fig. 2. $Th^{+/-}$ mice showed similar adaptation to cold exposure in BAT compared with $Th^{+/+}$ mice. A: The graphs represent the amount of dopamine or NA (ng/μg protein) after 6 h of cold exposure in BAT. B, C: Body weight and rectal temperature after cold exposure. D: Skin temperature surrounding BAT measured after 6 h of cold exposure. E: Energy expenditure was recorded during 4 h at both thermoneutrality and after 6 h of cold exposure (left and middle bars), as well as in the next night cycle as detailed in the graph (right bars). F–I: Quantitative RT-PCR of different thermogenic genes RNA expression in BAT. The data were normalized by *Tbp* RNA expression. All data were relative to $Th^{+/+}$ at 29°C. Data are mean ± SEM. n = 6/group in A, n = 10/group in B and C, n = 5–9/group in D and E, and n = 4–11/group in F–I. Unpaired *t*-test was used for catecholamine content analysis, and Mann-Whitney *U* test was used for gene expression analysis. A, F–I: $*P < 0.05$; $**P < 0.01$ (between $Th^{+/+}$ and $Th^{+/-}$ mice); $\#P < 0.05$; $\#\#P < 0.01$; $\#\#\#P < 0.001$ (between each genotype at 4°C and 29°C). E: $\#\#P < 0.01$; $\#\#\#P < 0.001$ [between light (15:30–19:30) or dark (19:30–08:30) periods after cold exposure (middle or right columns, respectively) versus light period (15:30–19:30) the day before cold exposure (left columns)].

T3 by DiO2 amplifies the cAMP response after adrenergic stimulation, thereby enhancing lipolysis and mitochondrial thermogenesis (35). In this context, we analyzed *Dio2* RNA levels and found similar basal levels at thermoneutrality in both genotypes, which increased to the same extent (about 100-fold) after cold exposure (supplemental Fig. S5B). Similarly, additional BAT-related gene expression analysis indicated no differences between the two genotypes after 6 h of cold exposure (supplemental Fig. S5C).

Th haploinsufficiency does not impact browning of iWAT

Prdm16 has been described to be essential in activating the thermogenic phenotype in inguinal subcutaneous depots (36). During cold acclimation, iWAT has been also reported to play a role in thermogenesis (37). The analysis of RNA levels of *Ucp1*, *Ppargc1a*, *Cidea*, and *Prdm16* in iWAT in 3 month old mice showed a similar expression pattern to that found in BAT at 29°C in the two genotypes (**Fig. 3A**; compare with Fig. 1F), a significant increase being detected exclusively in *Prdm16* in $Th^{+/-}$ mice (Fig. 3A). Moreover, upon cold exposure, the iWAT of *Th* heterozygous animals responded similarly to that of the controls, displaying comparable RNA levels of *Ucp1*, *Ppargc1a*, *Prdm16*, and *Cidea* genes (Fig. 3B–E), as well as levels of *Adrb3* and *Fgf21* (supplemental Fig. S6A, B).

Th haploinsufficiency increases FGF21 in BAT

After finding unaltered the key players in the thermogenic response in BAT and iWAT in $Th^{+/-}$ mice, we investigated possible factors that could compensate the catecholamine deficit. We hypothesized that unbalanced catecholamine levels may represent a stress with an impact on the expression of the batokine *Fgf21,* as occurred in the liver under lipotoxic conditions (38). As shown in **Fig. 4A**, significantly higher *Fgf21* RNA levels were found in BAT of $Th^{+/-}$ animals at 3 months of age at thermoneutral conditions. As occurred with other thermogenic genes, cold exposure increased BAT *Fgf21* expression to a similar extent in both genotypes of mice (Fig. 4A). Furthermore, plasma FGF21 levels were increased about 5-fold in $Th^{+/-}$ mice at thermoneutrality (Fig. 4B) in parallel to an elevated expression of *Fgf21* in the liver (Fig. 4C), the main source of circulating FGF21 (39). These results showed that, at thermoneutrality, $Th^{+/-}$ mice displayed an increase in both local BAT production and circulating levels of FGF21, suggesting a close relationship between the mild phenotype of *Th* haploinsufficency and the elevated *Fgf21* expression. Conversely, upon cold exposure plasma FGF21 and hepatic *Fgf21* RNA levels did not change in WT mice as described (40, 41), whereas both parameters decreased in $Th^{+/-}$ mice up to the levels of the WT. In BAT, FGF21 signals through heterocomplexes of the receptors bklotho (*Klb*) and FGFR1 (42). The analysis of the expression of both coreceptors at thermoneutrality and after cold exposure showed no differences in their RNA levels (Fig. 4D, E).

We next checked the timing of the onset of *Fgf21* upregulation. The analysis of BAT in e18.5 embryos showed

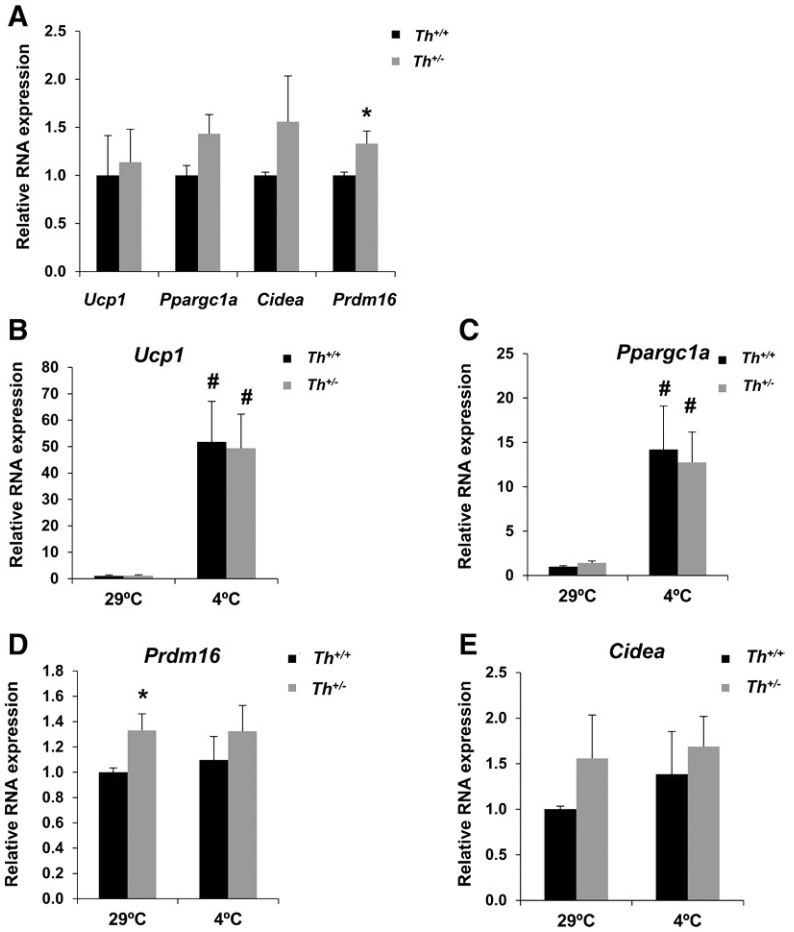

Fig. 3. $Th^{+/-}$ mice showed a similar adaptation to cold exposure in iWAT compared with $Th^{+/+}$ mice. A: Analysis by quantitative RT-PCR of different browning markers in iWAT at 29°C. All data were relative to RNA levels of $Th^{+/+}$. B–E: Quantitative RT-PCR of different thermogenic gene RNA expression in iWAT at 29°C and 4°C. All data were relative to $Th^{+/+}$ mice at 29°C. All expression data were normalized with *Tbp* RNA expression. Data are mean ± SEM. n = 4 or 5/group. Mann-Whitney *U* test was used. $*P < 0.05$ (between $Th^{+/+}$ and $Th^{+/-}$ mice); $\#P < 0.05$ (between each genotype at 4°C and 29°C).

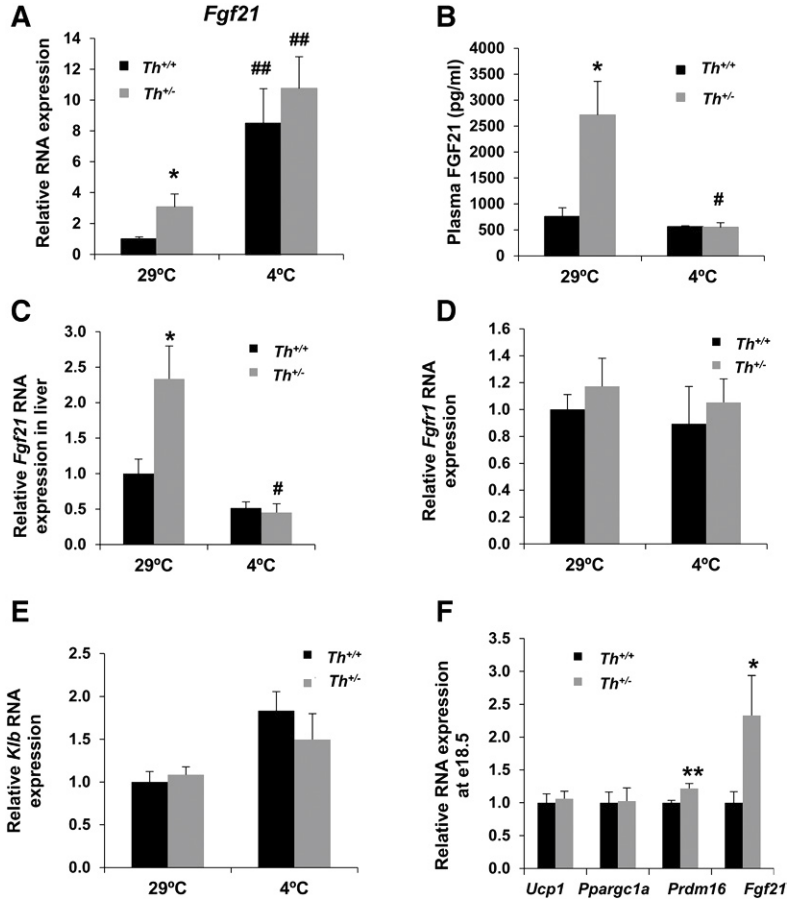

Fig. 4. *Th* haploinsufficiency increased *Fgf21* expression in BAT. A: Quantitative RT-PCR of *Fgf21* RNA expression in BAT at 29°C and 4°C. B: Content of FGF21 protein in plasma in thermoneutral and cold conditions measured by ELISA. C: Relative expression of *Fgf21* by quantitative RT-PCR analysis in livers at 29°C and 4°C. D, E: Relative expression of FGF21 coreceptors (*Fgfr1* and *Klb*) by quantitative RT-PCR analysis in BAT at 29°C and 4°C. All data were relative to RNA levels of $Th^{+/+}$ mice at 29°C. F: Quantitative RT-PCR of different browning markers RNA expression in BAT of e18.5 embryos. All data were relative to $Th^{+/+}$ animals. Data are mean ± SEM. n = 9 or 10/group in A, n = 9/group in B, n = 10/group in C, n = 4 or 5/group in D and E, and n = 12–20/group in F. All expression data were normalized with *Tbp* RNA expression. Mann-Whitney *U* test was used. *$P < 0.05$; **$P < 0.01$ (between $Th^{+/+}$ mice and $Th^{+/-}$ mice group); #$P < 0.05$; ##$P < 0.01$ (between each genotype at 4°C and 29°C).

higher levels of *Fgf21* RNA in the $Th^{+/-}$ embryos than in their WT littermates (Fig. 4F). Similarly, *Prdm16* RNA was increased at e18.5 in the $Th^{+/-}$ BAT, as described in adult mice. However, we did not observe differences in the RNA levels of the thermogenic-related genes *Ucp1* and *Ppargc1a*. Of note, a trend toward an increase in embryonic plasma and liver FGF21 content was detected in $Th^{+/-}$ embryos (supplemental Fig. S7A, B). In addition, the BAT of $Th^{+/-}$ old animals (15 months of age) showed a nearly significant increase in *Fgf21* RNA levels (supplemental Fig. S7C), reinforcing a possible role of this batokine in $Th^{+/-}$ mice.

$Th^{+/-}$ mice show increased BAT ER stress levels at thermoneutrality

To further explore a possible mechanism by which *Fgf21* expression was elevated in the BAT of $Th^{+/-}$ mice, we focused on endoplasmic reticulum (ER) stress, one of the well-known triggers of FGF21 expression (39, 43). The analysis of CHOP protein levels in BAT extracts showed a significant increase of this ER stress long-term marker in $Th^{+/-}$ mice at 3 months in thermoneutral conditions (**Fig. 5A**). However, in agreement with the absence of differences between both genotypes in *Fgf21* RNA levels in BAT after cold exposure, no differences in CHOP levels were found after cold challenge. Likewise, the relative phosphorylation of IRE1 and JNK, important signaling mediators in the unfolded protein response, was also increased in the BAT of $Th^{+/-}$ mice respect to the $Th^{+/-}$ control mice only at thermoneutrality (Fig. 5B, C).

Increased lipolytic capacity and TAG availability in the BAT of $Th^{+/-}$ mice

To get additional insight into the compensatory response of mice with reduced catecholamines during cold adaptation, we examined BAT lipolytic activity by the analysis of phosphorylation of the hormone-sensitive lipase (HSL) at the regulatory residue Ser-660. **Figure 6A** shows that although no differences were detected at thermoneutrality, HSL Ser-660 phosphorylation was significantly higher in the BAT of $Th^{+/-}$ mice at 3 months compared with that of the $Th^{+/+}$ controls after 6 h of cold exposure. This result indicated that a sustained lipolytic capacity of BAT in $Th^{+/-}$ mice was probably contributing to the activation of UCP-1. However, plasma glycerol and FFA levels were similar in both genotypes of mice (data not shown). To explain these results, we performed in vitro experiments using differentiated brown adipocytes previously characterized (23). As an experimental approach to mimic in vivo *Th* haploinsufficiency, brown adipocytes were stimulated with submaximal (0.1 μM) concentrations of NA for 4 h with or without a pretreatment with recombinant FGF21 (1 μg/ml) for 18 h. As shown in Fig. 6B, there was an increase in phospho-HSL in brown adipocytes pretreated with FGF21 prior to NA stimulation. Importantly, under these experimental conditions, a significant elevation was found in glycerol released to the culture medium (Fig. 6C) and, more importantly, in UCP-1 protein levels (Fig. 6D).

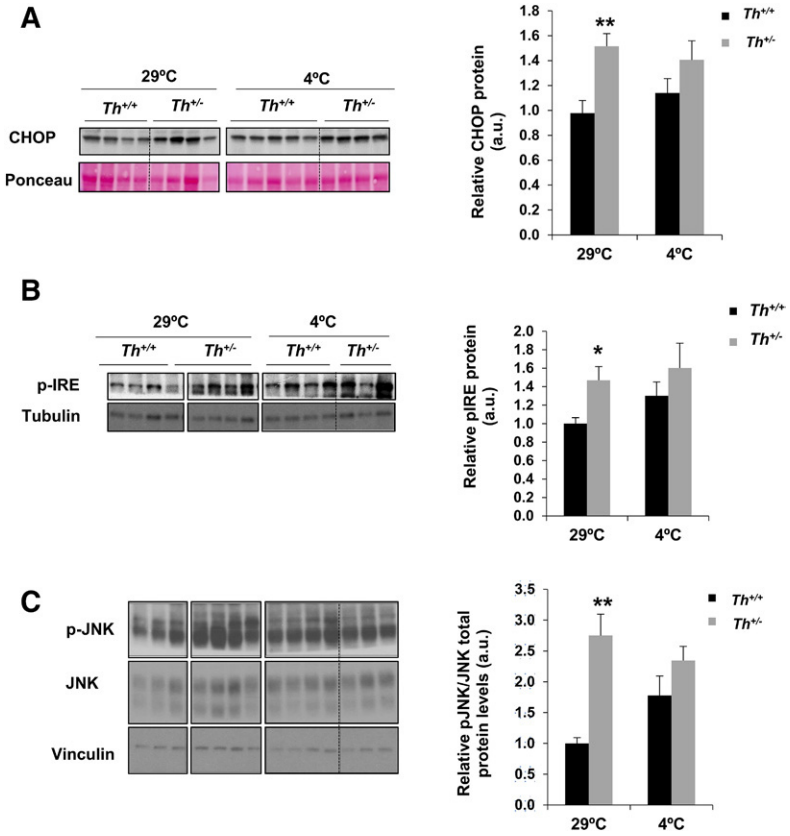

Fig. 5. The ER stress-mediated signaling was altered in BAT of $Th^{+/-}$ mice in thermoneutrality conditions. A: Western blot analysis and quantification of CHOP protein. Ponceau Red was used as a loading control. B, C: Western blot analysis and quantification of pIRE or pJNK, respectively. Tubulin, total JNK, and vinculin were used as loading controls. All data are relative to $Th^{+/+}$ mice densitometry at 29°C. Data are mean ± SEM. n = 4–10/group in A, and n = 3–10/group in B. Two-way ANOVA was used. $*P < 0.05$; $**P < 0.01$. a.u., arbitrary units.

To further investigate in detail the profile of different lipidic species in the two groups of mice, we performed a mass-spectrometry-based lipidomic study of total neutral lipid classes in BAT samples from mice at thermoneutral and cold conditions (**Tables 2** and **3** and **Fig. 7A**–D). Interestingly, at thermoneutrality, several FAs in TAG and DAG fractions were significantly elevated in $Th^{+/-}$ mice, suggesting that increased overall fat content, and likely lipotoxicity, which would lead to elevated ER stress in the BAT of $Th^{+/-}$ mice. Conversely, the levels of FFAs C16:0 (palmitic acid) and C18:0 (stearic acid) were reduced. The cholesteryl ester (CE) content showed no differences between the two genotypes (Fig. 7D). After cold exposure, the $Th^{+/-}$ animals maintained higher levels of TAG or DAG species compared with those of their WT littermates. In addition, the total amount of FFAs was higher in $Th^{+/-}$ BAT (Fig. 7C) compared with levels of the $Th^{+/+}$ BAT with significant increases in palmitic acid (Table 3).

DISCUSSION

Catecholamines are essential neurotransmitters for the maintenance of physiological homeostasis under basal and stress conditions. In BAT, catecholamines are responsible for the activation of nonshivering thermogenesis (5, 9). Also, dopamine has been shown to directly impact mitochondrial mass and thermogenesis in brown adipocytes (44). Whereas human pathologies with elevations of circulating catecholamines, such as pheochromocytoma, concur with excessive BAT activation (16, 45, 46), much less is known about the impact of reduced catecholamine biosynthesis in BAT functionality. The present work, using a murine preclinical model of global *Th* haploinsufficiency, has revealed an unexpectedly normal cold adaptation under reduced catecholamine availability. The early and life-long increase in FGF21 levels of $Th^{+/-}$ mice represents a potential new insight on the compensatory mechanisms that may operate in $Th^{+/-}$ BAT to ensure its full activation upon cold challenge.

The unique role of the sympathetic-mediated NA stimulation of BAT was highlighted by Lee et al. (10) showing that ablation of TH protein in BAT by denervation abolished UCP-1 induction during cold stress. More recently, a role of adipose tissue M2 macrophages or eosinophils as an additional catecholamine source in BAT or iWAT has been postulated (47–50), although controversies have also been raised regarding the contribution of these immune cells in secreting enough catecholamines to promote BAT activation or browning of iWAT (48). In our model, we found unexpected mild consequences of the global reduction of TH expression in BAT thermogenesis since $Th^{+/-}$ mice adapted normally to cold stress as manifested by the maintenance of rectal temperature, body weight, temperature of the skin surrounding BAT, and *Ucp1* induction. In particular, the significant increase in the expression of the thermogenic-related gene *Prdm16* that was detected in BAT of $Th^{+/-}$ mice suggests an early relationship between this master regulator of BAT development and TH. *Prdm16* has been previously described as a critical transcriptional

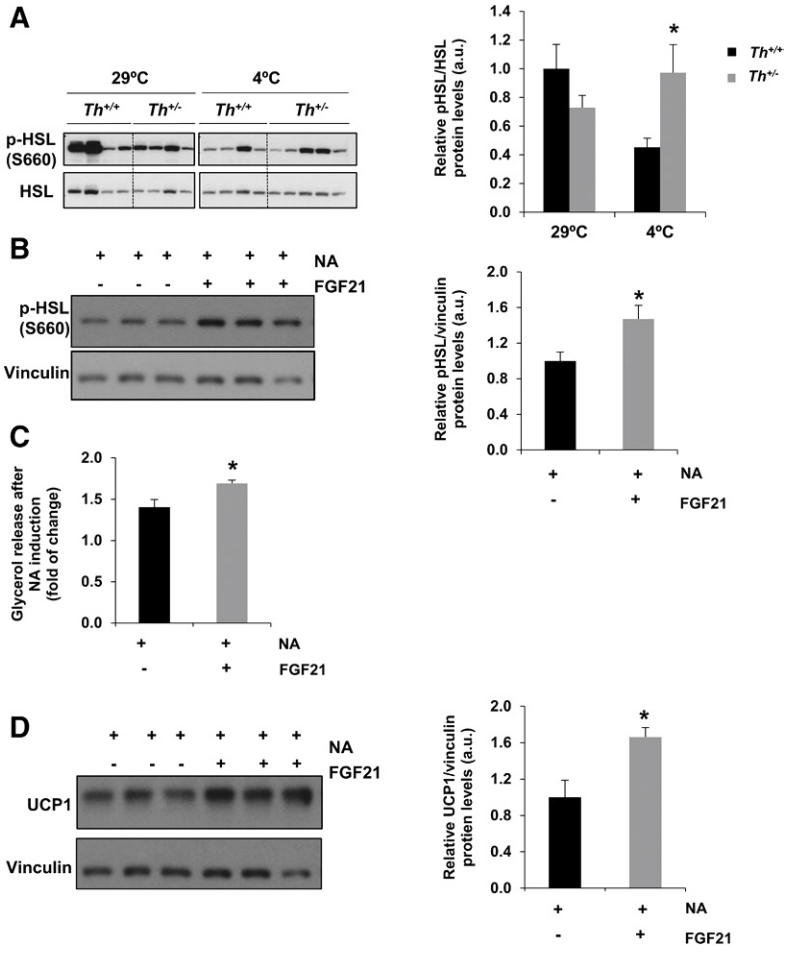

Fig. 6. Evaluation of phosphorylation of HSL in BAT of $Th^{+/+}$ and $Th^{+/-}$ mice and brown adipocytes stimulated with FGF21. A: Western blot analysis and quantification of phospho-HSL (S660) in BAT extracts. Total HSL was used as loading control. All data are relative to $Th^{+/+}$ mice densitometry at 29°C. B: Western blot analysis and quantification of phospho-HSL (S660) in differentiated brown adipocytes with or without FGF21 pretreatment (1 µg/ml for 18 h) before the addition of 0.1 µM NA for 4 h. Vinculin was used as a loading control. C: Quantification of glycerol release after NA stimulation under conditions described in B. D: UCP-1 protein levels under conditions described in B. Two-way ANOVA was used in Western blot analysis in A, and Mann-Whitney *U* test was used in B–D. $*P < 0.05$ (between $Th^{+/+}$ mice and $Th^{+/-}$ mice group or brown adipocytes pretreated or not with FGF21 and stimulated with NA between +FGF21 and –FGF21); $*P < 0.05$ (between each genotype). Data are mean ± SEM. n = 7–11/group in A, n = 5–7/group in B and D, and n = 3 independent experiments in C. a.u., arbitrary units.

regulator of thermogenesis that is essential for the differentiation of brown adipocytes, as well as for the browning process in beige fat cells (9, 51). A recent study has demonstrated that PRDM16 stabilizes the response to β3-adrenergic signaling to increase thermogenic gene expression and mitochondrial biogenesis in subcutaneous WAT by interacting with the transcription factor HLX (52). In agreement with these data, the iWAT of $Th^{+/-}$ mice showed an increase in *Prdm16* RNA levels, supporting the relevance of TH in the process of browning. These results were reinforced by the upregulation of *Prdm16* even in the embryonic BAT of $Th^{+/-}$ mice, indicating that during embryonic development, these mice have already activated compensatory mechanisms to overcome *Th* haploinsufficiency; *Prdm16* seems to be a relevant contributor to this phenotype. In fact, catecholamines are required to respond to stress during gestation. In this regard, it has been reported that *Th*-null mice die at midgestation due to cardiovascular failure (11, 12). This effect is likely a consequence of their inability to adapt to the gestational hypoxia (53). However, additional posttraslational modifications in PRDM16 such as sumoylation that primes its stabilization, as recently reported (54), cannot be excluded.

Beside changes in *Prdm16* gene expression, the largest changes found in BAT of $Th^{+/-}$ mice were detected in FGF21, which was significantly elevated under thermoneutral conditions compared with the $Th^{+/+}$ controls; this effect was maintained during aging. This batokine has been previously found to be increased under various situations including starvation, ketogenic diets, and overfeeding, as well as by deficiency or excess in dietary proteins and carbohydrates, respectively (43, 55). Although FGF21 is mainly synthetized and released by the liver (56), the BAT is another source of FGF21, where it has autocrine/paracrine functions related to upregulation of UCP-1 and thermogenesis (19, 57). We also found elevated FGF21 in the plasma from $Th^{+/-}$ mice, an effect that could be explained by the increased liver expression and secretion. Altogether, these results suggest that less TH availability induces regulatory mechanisms in BAT, likely mediated by *Prdm16* and/or *Fgf21,* which overall appear to compensate thermoregulatory changes and lead to normal adaptation to cold.

We next explored the possible molecular mechanisms that could explain the elevation of FGF21 in $Th^{+/-}$ mice. Several recent reports have demonstrated that the expression of *Fgf21* in the liver is induced by ER stress (58, 59). However, *Fgfr1* deficiency in WAT led to a sustained lipid droplet expansion and ER stress (42). In BAT, a direct relationship between ER stress and FGF21 levels has been well described under cold exposure or after birth during suckling (60). In agreement with the involvement of ER stress in the $Th^{+/-}$ phenotype, elevation of several ER stress markers was detected in the BAT of $Th^{+/-}$ mice at thermoneutrality, allowing us to speculate that ER stress in BAT,

TABLE 2. FA distribution profile of TAG, DAG, FFA, or CE in BAT from $Th^{+/+}$ and $Th^{+/-}$ mice

	Percent of $Th^{+/-}$ Content vs. $Th^{+/+}$ (29°C), %	Statistical Significance
TAG		
14:00	189.71	ns
16:0	175.58	***
16:1n-9	151.91	ns
16:1n-7	201.60	**
18:0	141.10	ns
18:1n-9	195.98	***
18:1n-7	22.24	ns
18:2n-6	164.42	**
18:3n-3	155.56	ns
20:0	187.69	ns
20:1n-9	230.35	ns
20:1n-7	70.53	ns
20:2n-6	319.92	ns
20:3n-6	281.93	ns
20:4n-6	153.95	ns
22:0	191.53	ns
22:1n-9	280.14	ns
CE		
16:0	99.99	ns
16:1n-9	87.56	ns
18:0	103.69	ns
18:1n-9	194.13	ns
DAG		
14:00	97.02	ns
16:0	144.27	***
16:1n-9	110.07	ns
16:1n-7	156.77	ns
18:0	132.05	ns
18:1n-9	137.05	*
18:2n-6	122.32	ns
FFA		
14:0	44.79	ns
16:0	56.52	***
16:1n-9	48.05	ns
16:1n-7	49.12	ns
18:0	64.87	***
18:1	73.91	ns
18:2	78.66	ns
20:0	36.71	ns
20:1n-9	66.85	ns
20:4n-6	57.76	ns
22:0	4.86	ns

Percentage of FAs in BAT of $Th^{+/-}$ versus $Th^{+/+}$ mice at 29°C. Data are mean ± SEM. n = 10 or 11/group. Two-way ANOVA was used. ns, not significant. *$P < 0.05$; **$P < 0.01$; ***$P < 0.001$.

TABLE 3. FA distribution profile of TAG, DAG, FFA, or CE in BAT from $Th^{+/+}$ and $Th^{+/-}$ mice

	Percent of $Th^{+/-}$ Content vs. $Th^{+/+}$ (4°C), %	Statistical Significance
TAG		
14:00	181.71	ns
16:0	173.28	***
16:1n-9	140.46	ns
16:1n-7	159.13	ns
18:0	188.45	ns
18:1n-9	175.79	***
18:1n-7	154.75	ns
18:2n-6	151.93	***
18:3n-3	136.76	ns
20:0	135.04	ns
20:1n-9	156.04	ns
20:1n-7	153.91	ns
20:3n-6	509.70	ns
20:4n-6	165.72	ns
22:0	71.27	ns
22:1n-9	618.31	ns
CE		
16:0	115.01	ns
16:1n-9	78.46	ns
18:0	103.95	ns
18:1n-9	100.63	ns
DAG		
14:0	105.54	ns
16:0	149.88	***
16:1n-9	45.13	ns
16:1n-7	143.62	ns
18:0	142.08	**
18:1n-9	141.47	***
18:2n-6	112.74	ns
20:0	110.29	ns
FFA		
14:0	121.51	ns
16:0	129.40	***
16:1n-9	142.10	ns
16:1n-7	148.56	ns
18:0	121.47	ns
18:1	166.77	ns
18:2	98.75	ns
20:0	73.58	ns
20:1n-9	99.28	ns
20:4n-6	58.98	ns
22:0	63.89	ns

Percentage of FAs in BAT of $Th^{+/-}$ versus $Th^{+/+}$ mice after 6 h exposure to cold at 4°C. Data are mean ± SEM. n = 10 or 11 per group. Two-way ANOVA was used. ns, not significant. *$P < 0.05$; * $P < 0.01$; ** $P < 0.001$.

probably due to reduced *Th* expression, may upregulate *Fgf*21.

Catecholamines are the inducers of lipolysis in adipose tissues. Zeng et al. (61) described that sympathetic denervation (or glucocorticoid administration) increased lipid accumulation in adipocytes due to defective lipolysis. In addition, lipolysis requires the activation of lipases such as adipose triglyceride lipase and HSL, as well as their stable association with the lipid droplets (62, 63). The analysis of phosphorylation of HSL at Ser-660, which is a direct indicator of its enzymatic activity, revealed elevations in the BAT of $Th^{+/-}$ mice after cold exposure, regardless of lower catecholamine levels. This response contrasted with decreased Ser-660 HSL phosphorylation in cold-exposed $Th^{+/+}$ mice, indicating that at least 6 h after cold exposure, the time at which the experiments were performed, the lipolytic activity due to HSL-mediated phosphorylation might be more sustained in the BAT of $Th^{+/-}$ mice, which would explain their maintained thermogenic capacity within a decreased catecholamine milieu. Interestingly, the stimulation of differentiated brown adipocytes with a submaximal dose of NA in the presence of FGF21 increased lipolysis and UCP-1 protein levels, reinforcing the in vivo data and indicating that the relationship between FGF21 and HSL might be important in this setting.

To find a possible explanation for such an effect, we analyzed TAG, DAG, and FFAs content in BAT from the two genotypes of mice. Again, substantial differences were found between genotypes. Decreased *Th* expression was accompanied by higher DAG and TAG content in BAT under basal conditions, and, importantly, TAG, DAG, and FFA content was increased after cold exposure compared with the levels of the $Th^{+/+}$ mice. This suggests an increased lipolysis rate, in accordance with the higher HSL phosphorylation. Interestingly, the differences observed in FFA levels

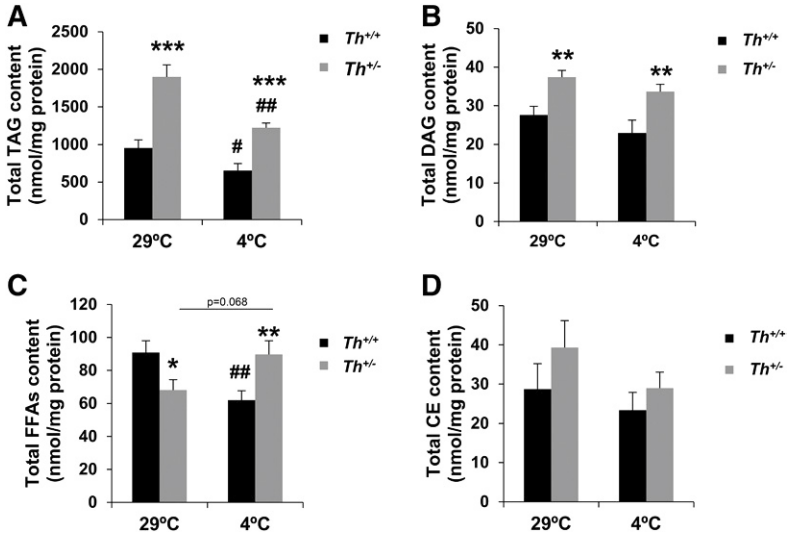

Fig. 7. TH heterozygous mice had different content of TAG, DAG, and FFAs at thermoneutrality or after cold exposure. The graph represents total content of TAG (A), DAG (B), FFAs (C), and CE (D) analyzed by lipidomics in BAT at 29°C or 4°C. The data were expressed by nmol/mg protein. Data are mean ± SEM. n = 10 or 11/group. Mann-Whitney *U* test was used in lipidomic analysis. *$P < 0.05$; **$P < 0.01$ (between $Th^{+/+}$ mice and $Th^{+/-}$ mice group); #$P < 0.05$; ##$P < 0.01$ (between each genotype at 4°C and 29°C).

upon cold exposure (i.e., significant increase in BAT from $Th^{+/-}$ mice was observed only for the saturated palmitic acid) suggest that BAT may adapt to temperature changes by modifying the ratio saturated versus unsaturated/polyunsaturated FFAs within neutral lipids via selective lipolysis. Thus, the loosening of acyl chain packing within TAG and DAG may provide BAT with a mechanism to finely adjust to temperature changes, as needed. These results suggest a more rapid replenishment and remodeling of fat stores in the lipid droplets in the BAT of $Th^{+/-}$ mice. In addition, the increased levels of highly lipotoxic species, such as DAG, might explain the existence of lipotoxicity and, subsequently, ER stress in *Th* haploinsufficiency. These complex mechanisms are likely to be necessary to respond to the stress of cold exposure in conditions of decreased *Th* expression because, as stated above, $Th^{+/-}$ mice adapted to cold with a similar pattern of thermogenic-related gene expression, body weight, and rectal and skin surrounding BAT temperature as the $Th^{+/+}$ mice. This adaptation may also be facilitated by elevated lipolytic substrates DAG and TAG under basal conditions, thereby yielding more availability of FFAs that ultimately are the fuels for UCP-1 activation in BAT (64). In fact, the histological analysis revealed an increase in fat (white) area in BAT from $Th^{+/-}$ mice at both thermoneutrality and cold conditions. Moreover, the lack of differences in plasma levels of FFAs and glycerol content between the two genotypes of mice (results not shown) could indicate that the FFAs resulting from lipolysis are being burned in the brown adipocytes as fuels generating the proton gradient in the mitochondria, rather than being exported to the circulation.

In summary, our results suggest the existence of an inverse relationship between *Th* expression and *Prdm16* and *Fgf21* in BAT under basal conditions that might operate under stress conditions in $Th^{+/-}$ mice to maintain BAT functionality/homeostasis. Thus, in a situation of *Th* haploinsufficiency, the elevation in FGF21, probably as a result of the subsequent lipotoxic-induced ER stress, together with the elevation in PRDM16 might ensure a normal response to cold exposure of BAT as well as iWAT. This compensation is likely facilitated by the higher content of DAG and TAG and increased activity of HSL in BAT from $Th^{+/-}$ mice, yielding more availability of FFAs that ultimately are the fuels for UCP-1 activation and thermogenesis. This evidence indicates a new mechanism for cold adaptation in a context of low adrenergic signaling, that may be therapeutically relevant. However, further research is needed to unravel whether additional intermediate factors are involved.

The authors thank personnel from the Centro de Investigaciones Biológicas (Madrid), A. Robles for technical assistance, and M. T. Seisdedos for assistance with confocal microscopy. The authors acknowledge the valuable input of F. Villarroya (University of Barcelona) in the discussion of the results.

REFERENCES

1. Lowell, B. B., and B. M. Spiegelman. 2000. Towards a molecular understanding of adaptive thermogenesis. *Nature.* **404:** 652–660.
2. Cinti, S. 2012. The adipose organ at a glance. *Dis. Models Mechanisms.* **5:** 588–594.
3. Carobbio, S., V. Pellegrinelli, and A. Vidal-Puig. 2017. Adipose tissue function and expandability as determinants of lipotoxicity and the metabolic syndrome. *In* Obesity and Lipotoxicity. A. B. Engin and A. Engin, editors. Springer International Publishing, Cham, Switzerland. **960:** 161–196.
4. Bhatt, P. S., W. S. Dhillo, and V. Salem. 2017. Human brown adipose tissue—function and therapeutic potential in metabolic disease. *Curr. Opin. Pharmacol.* **37:** 1–9.
5. Wankhade, U. D., M. Shen, H. Yadav, and K. M. Thakali. 2016. Novel browning agents, mechanisms, and therapeutic potentials of brown adipose tissue. *BioMed Res. Int.* **2016:** 2365609.
6. Chu, D-T., and B. Gawronska-Kozak. 2017. Brown and brite adipocytes: same function, but different origin and response. *Biochimie.* **138:** 102–105.
7. Lee, P., J. T. Zhao, M. M. Swarbrick, G. Gracie, R. Bova, J. R. Greenfield, J. Freund, and K. K. Y. Ho. 2011. High prevalence of brown adipose tissue in adult humans. *J. Clin. Endocrinol. Metab.* **96:** 2450–2455.
8. Bartelt, A., O. T. Bruns, R. Reimer, H. Hohenberg, H. Ittrich, K. Peldschus, M. G. Kaul, U. I. Tromsdorf, H. Weller, C. Waurisch, et al. 2011. Brown adipose tissue activity controls triglyceride clearance. *Nat. Med.* **17:** 200–205.
9. Bargut, T. C. L., M. B. Aguila, and C. A. Mandarim-de-Lacerda. 2016. Brown adipose tissue: updates in cellular and molecular biology. *Tissue Cell.* **48:** 452–460.

10. Lee, Y-H., A. P. Petkova, A. A. Konkar, and J. G. Granneman. 2015. Cellular origins of cold-induced brown adipocytes in adult mice. *FASEB J.* **29:** 286–299.
11. Kobayashi, K., S. Morita, H. Sawada, T. Mizuguchi, K. Yamada, I. Nagatsu, T. Hata, Y. Watanabe, K. Fujita, and T. Nagatsu. 1995. Targeted disruption of the tyrosine hydroxylase locus results in severe catecholamine depletion and perinatal lethality in mice. *J. Biol. Chem.* **270:** 27235–27243.
12. Zhou, Q-Y., C. J. Quaife, and R. D. Palmiter. 1995. Targeted disruption of the tyrosine hydroxylase gene reveals that catecholamines are required for mouse fetal development. *Nature.* **374:** 640–643.
13. Rios, M., B. Habecker, T. Sasaoka, G. Eisenhofer, H. Tian, S. Landis, D. Chikaraishi, and S. Roffler-Tarlov. 1999. Catecholamine synthesis is mediated by tyrosinase in the absence of tyrosine hydroxylase. *J. Neurosci.* **19:** 3519–3526.
14. Vázquez, P., A. M. Robles, F. de Pablo, and C. Hernández-Sánchez. 2014. Non-neural tyrosine hydroxylase, via modulation of endocrine pancreatic precursors, is required for normal development of beta cells in the mouse pancreas. *Diabetologia.* **57:** 2339–2347.
15. Gamella-Pozuelo, L., M. T. Grande, M. Clemente-Lorenzo, C. Murillo-Gómez, F. De Pablo, J. M. López-Novoa, and C. Hernández-Sánchez. 2017. Tyrosine hydroxylase haploinsufficiency prevents age-associated arterial pressure elevation and increases half-life in mice. *Biochim. Biophys. Acta Mol. Basis Dis.* **1863:** 113–120.
16. Nagano, G., H. Ohno, K. Oki, K. Kobuke, T. Shiwa, M. Yoneda, and N. Kohno. 2015. Activation of classical brown adipocytes in the adult human perirenal depot is highly correlated with PRDM16–EHMT1 complex expression. *PLoS One.* **10:** e0122584.
17. Tümer, N., and J. S. Larochelle. 1995. Tyrosine hydroxylase expression in rat adrenal medulla: Influence of age and cold. *Pharmacol. Biochem. Behav.* **51:** 775–780.
18. Vargovic, P., G. Manz, and R. Kvetnansky. 2016. Continuous cold exposure induces an anti-inflammatory response in mesenteric adipose tissue associated with catecholamine production and thermogenin expression in rats. *Endocr. Regul.* **50:** 137–144.
19. Villarroya, F., R. Cereijo, J. Villarroya, and M. Giralt. 2017. Brown adipose tissue as a secretory organ. *Nat. Rev. Endocrinol.* **13:** 26–35.
20. Xie, T., and P. S. Leung. 2017. Fibroblast growth factor 21: a regulator of metabolic disease and health span. *Am. J. Physiol. Endocrinol. Metab.* **313:** E292–E302.
21. Liu, L., C. Zhao, Y. Yang, X. Kong, T. Shao, L. Ren, X. Zhuang, B. Yin, G. Dryden, C. McClain, et al. 2017. Fibroblast growth factor 21 deficiency attenuates experimental colitis-induced adipose tissue lipolysis. *Gastroenterol. Res. Pract.* **2017:** 3089378.
22. Gimeno, R. E., and D. E. Moller. 2014. FGF21-based pharmacotherapy – potential utility for metabolic disorders. *Trends Endocrinol. Metab.* **25:** 303–311.
23. García-Casarrubios, E., C. de Moura, A. I. Arroba, N. Pescador, M. Calderon-Dominguez, L. Garcia, L. Herrero, D. Serra, S. Cadenas, F. Reis, et al. 2016. Rapamycin negatively impacts insulin signaling, glucose uptake and uncoupling protein-1 in brown adipocytes. *Biochim. Biophys. Acta.* **1861:** 1929–1941.
24. Folch, J., M. Lees, and G. H. S. Stanley. 1957. A simple method for the isolation and purification of total lipides from animal tissues. *J. Biol. Chem.* **226:** 497–509.
25. Diez, E., J. Balsinde, M. Aracil, and A. Schüller. 1987. Ethanol induces release of arachidonic acid but not synthesis of eicosanoids in mouse peritoneal macrophages. *Biochim. Biophys. Acta.* **921:** 82–89.
26. Guijas, C., G. Pérez-Chacón, A. M. Astudillo, J. M. Rubio, L. Gilde-Gómez, M. A. Balboa, and J. Balsinde. 2012. Simultaneous activation of p38 and JNK by arachidonic acid stimulates the cytosolic phospholipase A2-dependent synthesis of lipid droplets in human monocytes. *J. Lipid Res.* **53:** 2343–2354.
27. Guijas, C., C. Meana, A. M. Astudillo, M. A. Balboa, and J. Balsinde. 2016. Foamy monocytes Are enriched in cis-7-hexadecenoic fatty acid (16:1n-9), a possible biomarker for early detection of cardiovascular disease. *Cell Chem. Biol.* **23:** 689–699.
28. Martínez de Morentin, P. B., I. González-García, L. Martins, R. Lage, D. Fernández-Mallo, N. Martínez-Sánchez, F. Ruíz-Pino, J. Liu, D. A. Morgan, L. Pinilla, et al. 2014. Estradiol regulates brown adipose tissue thermogenesis via hypothalamic AMPK. *Cell Metab.* **20:** 41–53.
29. Martínez-Sánchez, N., P. Seoane-Collazo, C. Contreras, L. Varela, J. Villarroya, E. Rial-Pensado, X. Buqué, I. Aurrekoetxea, T. C. Delgado, R. Vázquez-Martínez, et al. 2017. Hypothalamic AMPK-ER stress-JNK1 axis mediates the central actions of thyroid hormones on energy balance. *Cell Metab.* **26:** 212–229.e12.
30. Festuccia, W. T., P-G. Blanchard, T. B. Oliveira, J. Magdalon, V. A. Paschoal, D. Richard, and Y. Deshaies. 2012. PPARγ activation attenuates cold-induced upregulation of thyroid status and brown adipose tissue PGC-1α and D2. *Am. J. Physiol. Regul. Integr. Comp. Physiol.* **303:** R1277.
31. Vatner, D. E., S. F. Vatner, J. Nejima, N. Uemura, E. E. Susanni, T. H. Hintze, and C. J. Homcy. 1989. Chronic norepinephrine elicits desensitization by uncoupling the beta-receptor. *J. Clin. Invest.* **84:** 1741–1748.
32. Granneman, J. G. 1992. Effects of agonist exposure on the coupling of beta 1 and beta 3 adrenergic receptors to adenylyl cyclase in isolated adipocytes. *J. Pharmacol. Exp. Ther.* **261:** 638.
33. Bengtsson, T., K. Redegren, A. D. Strosberg, J. Nedergaard, and B. Cannon. 1996. Down-regulation of β3 adrenoreceptor gene expression in brown fat cells is transient and recovery is dependent upon a short-lived protein factor. *J. Biol. Chem.* **271:** 33366–33375.
34. López, M., C. V. Alvarez, R. Nogueiras, and C. Diéguez. 2013. Energy balance regulation by thyroid hormones at central level. *Trends Mol. Med.* **19:** 418–427.
35. Obregon, M-J. 2014. Adipose tissues and thyroid hormones. *Front. Physiol.* **5:** 479.
36. Seale, P. 2015. Transcriptional regulatory circuits controlling brown fat development and activation. *Diabetes.* **64:** 2369–2375.
37. Keipert, S., M. Kutschke, M. Ost, T. Schwarzmayr, E. M. van Schothorst, D. Lamp, L. Brachthäuser, I. Hamp, S. E. Mazibuko, S. Hartwig, et al. 2017. Long-term cold adaptation does not require FGF21 or UCP1. *Cell Metab.* **26:** 437–446.e5.
38. Maratos-Flier, E. 2017. Fatty liver and FGF21 physiology. *Exp. Cell Res.* **360:** 2–5.
39. Gómez-Sámano, M. Á., M. Grajales-Gómez, J. M. Zuarth-Vázquez, M. F. Navarro-Flores, M. Martínez-Saavedra, Ó. A. Juárez-León, M. G. Morales-García, V. M. Enríquez-Estrada, F. J. Gómez-Pérez, and D. Cuevas-Ramos. 2017. Fibroblast growth factor 21 and its novel association with oxidative stress. *Redox Biol.* **11:** 335–341.
40. Hondares, E., R. Iglesias, A. Giralt, F. J. Gonzalez, M. Giralt, T. Mampel, and F. Villarroya. 2011. Thermogenic activation induces FGF21 expression and release in brown adipose tissue. *J. Biol. Chem.* **286:** 12983–12990.
41. Flachs, P., K. Adamcova, P. Zouhar, C. Marques, P. Janovska, I. Viegas, J. G. Jones, K. Bardova, M. Svobodova, J. Hansikova, et al. 2017. Induction of lipogenesis in white fat during cold exposure in mice: link to lean phenotype. *Int. J. Obes. (Lond.).* **41:** 372–380.
42. Ye, M., W. Lu, X. Wang, C. Wang, J. L. Abbruzzese, G. Liang, X. Li, and Y. Luo. 2016. FGF21-FGFR1 coordinates phospholipid homeostasis, lipid droplet function, and ER stress in obesity. *Endocrinology.* **157:** 4754–4769.
43. Jiang, S., C. Yan, Q-c. Fang, M-l. Shao, Y-l. Zhang, Y. Liu, Y-p. Deng, B. Shan, J-q. Liu, H-t. Li, et al. 2014. Fibroblast growth factor 21 is regulated by the IRE1Î±-XBP1 branch of the unfolded protein response and counteracts endoplasmic reticulum stress-induced hepatic steatosis. *J. Biol. Chem.* **289:** 29751–29765.
44. Kohlie, R., N. Perwitz, J. Resch, S. M. Schmid, H. Lehnert, J. Klein, and K. A. Iwen. 2017. Dopamine directly increases mitochondrial mass and thermogenesis in brown adipocytes. *J. Mol. Endocrino.* **58**: 57–66.
45. Wang, Q., M. Zhang, G. Ning, W. Gu, T. Su, M. Xu, B. Li, and W. Wang. 2011. Brown adipose tissue in humans is activated by elevated plasma catecholamines levels and is inversely related to central obesity. *PLoS One.* **6:** e21006.
46. Frontini, A., A. Vitali, J. Perugini, I. Murano, C. Romiti, D. Ricquier, M. Guerrieri, and S. Cinti. 2013. White-to-brown transdifferentiation of omental adipocytes in patients affected by pheochromocytoma. *Biochim. Biophys. Acta.* **1831:** 950–959.
47. Qiu, Y., K. D. Nguyen, J. I. Odegaard, X. Cui, X. Tian, R. M. Locksley, R. D. Palmiter, and A. Chawla. 2014. Eosinophils and type 2 cytokine signaling in macrophages orchestrate development of functional beige fat. *Cell.* **157:** 1292–1308.
48. Fischer, K., H. H. Ruiz, K. Jhun, B. Finan, D. J. Oberlin, V. van der Heide, A. V. Kalinovich, N. Petrovic, Y. Wolf, C. Clemmensen, et al. 2017. Alternatively activated macrophages do not synthesize catecholamines or contribute to adipose tissue adaptive thermogenesis. *Nat. Med.* **23:** 623–630.
49. Nguyen, K. D., Y. Qiu, X. Cui, Y. P. S. Goh, J. Mwangi, T. David, L. Mukundan, F. Brombacher, R. M. Locksley, and A. Chawla. 2011. Alternatively activated macrophages produce catecholamines to sustain adaptive thermogenesis. *Nature.* **480**: 104–108.
50. Qiu, Y., K. D. Nguyen, J. I. Odegaard, X. Cui, X. Tian, R. M. Locksley, R. D. Palmiter, and A. Chawla. 2014. Eosinophils and type

2 cytokine signaling in macrophages orchestrate development of functional beige fat. *Cell.* **157:** 1292–1308.
51. Seale, P., S. Kajimura, W. Yang, S. Chin, L. M. Rohas, M. Uldry, G. Tavernier, D. Langin, and B. M. Spiegelman. 2007. Transcriptional control of brown fat determination by PRDM16. *Cell Metab.* **6:** 38–54.
52. Huang, L., D. Pan, Q. Chen, L. J. Zhu, J. Ou, M. Wabitsch, and Y-X. Wang. 2017. Transcription factor Hlx controls a systematic switch from white to brown fat through Prdm16-mediated co-activation. *Nat. Commun.* **8:** 68.
53. Ream, M. A., R. Chandra, M. Peavey, A. M. Ray, S. Roffler-Tarlov, H-G. Kim, W. C. Wetsel, H. A. Rockman, and D. M. Chikaraishi. 2008. High oxygen prevents fetal lethality due to lack of catecholamines. *Am. J. Physiol. Regul. Integr. Comp. Physiol.* **295:** R942–R953.
54. Chen, Q., L. Huang, D. Pan, L. J. Zhu, and Y-X. Wang. 2018. Cbx4 sumoylates Prdm16 to regulate adipose tissue thermogenesis. *Cell Reports.* **22:** 2860–2872.
55. Staiger, H., M. Keuper, L. Berti, M. Hrabě de Angelis, and H-U. Häring. 2017. Fibroblast growth factor 21—Metabolic role in mice and men. *Endocr. Rev.* **38:** 468–488.
56. Liang, Q., L. Zhong, J. Zhang, Y. Wang, S. R. Bornstein, C. R. Triggle, H. Ding, K. S. L. Lam, and A. Xu. 2014. FGF21 maintains glucose homeostasis by mediating the cross talk between liver and brain during prolonged fasting. *Diabetes.* **63:** 4064.
57. Cereijo, R., J. Villarroya, and F. Villarroya. 2015. Non-sympathetic control of brown adipose tissue. *Int. J. Obes. Suppl.* **5:** S40–S44.
58. Schaap, F. G., A. E. Kremer, W. H. Lamers, P. L. M. Jansen, and I. C. Gaemers. 2013. Fibroblast growth factor 21 is induced by endoplasmic reticulum stress. *Biochimie.* **95:** 692–699.
59. Yang, C., W. Lu, T. Lin, P. You, M. Ye, Y. Huang, X. Jiang, C. Wang, F. Wang, M-H. Lee, et al. 2013. Activation of liver FGF21 in hepatocarcinogenesis and during hepatic stress. *BMC Gastroenterol.* **13:** 67.
60. Hondares, E., M. Rosell, F. J. Gonzalez, M. Giralt, R. Iglesias, and F. Villarroya. 2010. Hepatic FGF21 expression is induced at birth via PPARα in response to milk intake and contributes to thermogenic activation of neonatal brown fat. *Cell Metab.* **11:** 206–212.
61. Zeng, X., M. P. Jedrychowski, Y. Chen, S. Serag, G. G. Lavery, S. P. Gygi, and B. M. Spiegelman. 2016. Lysine-specific demethylase 1 promotes brown adipose tissue thermogenesis via repressing glucocorticoid activation. *Genes Dev.* **30:** 1822–1836.
62. Moore, H-P. H., R. B. Silver, E. P. Mottillo, D. A. Bernlohr, and J. G. Granneman. 2005. Perilipin targets a novel pool of lipid droplets for lipolytic attack by hormone-sensitive lipase. *J. Biol. Chem.* **280:** 43109–43120.
63. Holm, C. 2003. Molecular mechanisms regulating hormone-sensitive lipase and lipolysis. *Biochem. Soc. Trans.* **31:** 1120.
64. Townsend, K., and Y-H. Tseng. 2012. Brown adipose tissue: recent insights into development, metabolic function and therapeutic potential. *Adipocyte.* **1:** 13–24.